

Article

Numerical Simulation for Fractional-Order Bloch Equation Arising in Nuclear Magnetic Resonance by Using the Jacobi Polynomials

Harendra Singh¹ and H. M. Srivastava^{2,3,4,*} 

¹ Department of Mathematics, Post-Graduate College, Ghazipur 233001, Uttar Pradesh, India; harendra059@gmail.com

² Department of Mathematics and Statistics, University of Victoria, Victoria, BC V8W 3R4, Canada

³ Department of Medical Research, China Medical University Hospital, China Medical University, Taichung 40402, Taiwan

⁴ Department of Mathematics and Informatics, Azerbaijan University, 71 Jeyhun Hajibeyli Street, Baku AZ1007, Azerbaijan

* Correspondence: harimsri@math.uvic.ca

Received: 17 March 2020; Accepted: 13 April 2020; Published: 20 April 2020



Abstract: In the present paper, we numerically simulate fractional-order model of the Bloch equation by using the Jacobi polynomials. It arises in chemistry, physics and nuclear magnetic resonance (NMR). It also arises in magnetic resonance imaging (MRI) and electron spin resonance (ESR). It is used for purity determination, provided that the molecular weight and structure of the compound is known. It can also be used for structural determination. By the study of NMR, chemists can determine the structure of many compounds. The obtained numerical results are compared and simulated with the known solutions. Accuracy of the proposed method is shown by providing tables for absolute errors and root mean square errors. Different orders of the time-fractional derivatives results are illustrated by using figures.

Keywords: fractional-order Bloch equation; nuclear magnetic resonance (NMR); magnetic resonance imaging (MRI); electron spin resonance (ESR); Jacobi polynomials

1. Introduction

The Bloch equation is a system of differential equations. It is mainly valuable for studying expensive biological samples like RNA, DNA, proteins and nucleic acids. It has many real-life applications like process control, liquid media, petrochemical plants and process optimization in oil refineries. Surface magnetic resonance is based on the principle of NMR, and the measurements can be used to indirectly estimate the water content of the saturated and unsaturated zones. The standard system of Bloch equations is given as follows:

$$\begin{aligned}\frac{dN_x(t)}{dt} &= w_0 N_y(t) - \frac{N_x(t)}{T_2} \\ \frac{dN_y(t)}{dt} &= w_0 N_x(t) - \frac{N_y(t)}{T_2}\end{aligned}\quad (1)$$

$$\frac{dN_z(t)}{dt} = \frac{N_0 - N_z(t)}{T_1},$$

with the initial conditions $N_x(0) = a_1$, $N_y(0) = a_2$ and $N_z(0) = a_3$.

Here $N_x(t)$, $N_y(t)$ and $N_z(t)$ denote the system magnetisation in x , y and z components, respectively; w_0 is the resonant frequency given by the Larmor relationship $w_0 = \gamma M_0$, where

M_0 is the static magnetic field in z -component, N_0 is the equilibrium magnetisation, T_1 and T_2 are the spin-lattice and spin-spin relaxation time, respectively, and a_1 , a_2 and a_3 are real constants. The analytical solution of Equation (1) is given by

$$\begin{aligned} N_x(t) &= e^{-\frac{t}{T_2}} \left(N_x(0) \cos w_0 t + N_y(0) \sin w_0 t \right) \\ N_y(t) &= e^{-\frac{t}{T_2}} \left(N_y(0) \cos w_0 t - N_x(0) \sin w_0 t \right) \\ N_z(t) &= N_z(0) e^{-\frac{t}{T_1}} + N_0 \left(1 - e^{-\frac{t}{T_1}} \right) \end{aligned} \tag{2}$$

Real-life applications of fractional calculus are in subjects like biology [1], viscoelasticity [2–4], signal processing [5], control theory [6], fluid dynamics [7]. For more details, the reader should refer to [8]. There are many magnetic resonance systems which are modelled by the fractional-order Bloch equation, and it is well known that the fractional-order derivatives are non-local in nature. Therefore, we will replace the integer-order Bloch equation by the fractional-order Bloch equation with a view to further understand the resulting magnetic resonance systems. Therefore, we replace the integer-order time-derivative by the non-integer-order time-derivative:

$$\begin{aligned} \frac{d^\alpha N_x(t)}{dt^\alpha} &= w_0 N_y(t) - \frac{N_x(t)}{T_2} \\ \frac{d^\beta N_y(t)}{dt^\beta} &= w_0 N_x(t) - \frac{N_y(t)}{T_2} \\ \frac{d^\gamma N_z(t)}{dt^\gamma} &= \frac{N_0 - N_z(t)}{T_1}, \end{aligned} \tag{3}$$

where $0 < \alpha, \beta, \gamma \leq 1$.

The non-integer-order derivative is in the Liouville–Caputo (LC) sense. The LC non-integer-order derivative of order β is defined as follows [8]:

$$D^\beta f(x) = I^{l-\beta} D^l f(x) = \frac{1}{\Gamma(l-\beta)} \int_0^x (x-t)^{l-\beta-1} \frac{d^l}{dt^l} f(t) dt, \quad l-1 < \beta < l, \quad x > 0.$$

In this paper, we are considering that $\beta \in (0, 1)$; therefore, we will take $l = 1$. The time-fractional derivatives play a key role upsetting the spin dynamics defined by the Bloch equations in Equation (3) (see [9,10]). The magnetic resonance components of the magnetisation are identified in the initial state of the system, and hence, these should be visibly predictable. The physical meaning of the non-integer order Bloch equations can be understood in the basic preparation of the non-integer-order Schrödinger equation.

Bloch equations in NMR can be simulated numerically and analytically (see, for details, [11–16]). The time-fractional order Bloch equation having fractional derivative in Caputo sense is solved in [17]. Recently, Kumar et al. [18] solved fractional-order Bloch equation by using homotopy perturbation method (HPM). Use has been made of operational matrix method with Legendre polynomials in [19] and with the Laguerre polynomials in [20] for the solution of this equation. In [21], this equation was solved numerically by using the iterative method. Furthermore, in [22], by using numerical approximation, a special class of this equation, namely the fuzzy time-fractional Bloch equation, was solved. In this paper we propose to solve the fractional-order Bloch equation by using the Jacobi polynomials. Some developments on orthogonal approximations can be found in [23–30]. Some introductory overview and recent development of fractional calculus can be seen in [31]. In this method, we get unknown coefficients for the approximated parameter in the model and, by the use of these coefficients, we obtain approximate solutions of the fractional-order Bloch equation in NMR.

2. Preliminaries

The Jacobi polynomial of degree i on $[0, 1]$ is given by [28]

$$\sigma_i(t) = \sum_{k=0}^i (-1)^{i-k} \frac{\Gamma(i+b+1)\Gamma(i+k+a+b+1)}{\Gamma(k+b+1)\Gamma(i+a+b+1)(i-k)!k!} t^k \tag{4}$$

The orthogonal property of the Jacobi polynomials with respect to the weight function $w^{(a,b)}(t) = (1-t)^a t^b$ is given by

$$\int_0^1 \sigma_n(t)\sigma_m(t)w^{(a,b)}(t)dt = v_n^{a,b} \delta_{mn} \tag{5}$$

where δ_{mn} is Kronecker delta function and

$$v_n^{a,b} = \frac{\Gamma(n+a+1)\Gamma(n+b+1)}{(2n+a+b+1)n!\Gamma(n+a+b+1)} \tag{6}$$

A function $f \in L^2[0, 1]$, with $|f''(t)| \leq Q$, can be expanded as follows:

$$f(t) = \lim_{n \rightarrow \infty} \sum_{i=0}^n c_i \sigma_i(t), \tag{7}$$

where $c_i = \frac{1}{v_i^{a,b}} \int_0^1 \sigma_i(t)f(t)w^{(a,b)}(t)dt$.

Equation (7), for finite dimensional approximation, is written in the following form:

$$f \cong \sum_{i=0}^m c_i \sigma_i(t) = C^T q_m(t), \tag{8}$$

where C and $q_m(t)$ are $(m+1) \times 1$ matrices given by $C = [c_0, c_1, \dots, c_m]^T$ and $q_m(t) = [\sigma_0, \sigma_1, \dots, \sigma_m]^T$.

Theorem 1. If $q_n(t) = [\sigma_0, \sigma_1, \dots, \sigma_n]^T$ denotes the shifted Jacobi vector and if $v > 0$, then $I^v \sigma_i(t) = I^{(v)} q_n(t)$, where $I^{(v)} = (u(i, j))$, is the $(n+1) \times (n+1)$ operational matrix of fractional integral of order v , and its (i, j) th entry is given by

$$u(i, j) = \sum_{k=0}^i \sum_{l=0}^j (-1)^{i+j-k-l} \frac{\Gamma(a+1)\Gamma(i+b+1)\Gamma(i+k+a+b+1)\Gamma(j+l+a+b+1)\Gamma(v+k+l+a+b+1)(2j+a+b+1)j!}{(i-k)!(j-l)!(l)! \Gamma(k+b+1)\Gamma(i+a+b+1)\Gamma(v+k+1)\Gamma(j+a+1)\Gamma(l+b+1)\Gamma(k+l+v+a+b+1)} \tag{9}$$

Proof. Please see [28]. □

3. Construction of Algorithm

In this section, we construct an algorithm to get the approximate solution of the Bloch equation. Using this algorithm, we can then obtain magnetisation in each direction.

Let us take the following approximations:

$$\frac{d^\alpha N_x(t)}{dt^\alpha} = C_1^T q(t), \quad \frac{d^\beta N_y(t)}{dt^\beta} = C_2^T q(t), \quad \frac{d^\gamma N_z(t)}{dt^\gamma} = C_3^T q(t), \tag{10}$$

and

$$N_x(0) = L^T q(t), \quad N_y(0) = M^T q(t), \quad N_z(0) = N^T q(t), \quad \frac{N_0}{T_1} = O^T q(t). \tag{11}$$

From Equations (10) and (11), we can write

$$N_x(t) = C_1^T I^{(\alpha)} q(t) + L^T q(t), \tag{12}$$

$$N_y(t) = C_2^T I^{(\beta)} q(t) + M^T q(t), \tag{13}$$

$$N_z(t) = C_3^T I^{(\gamma)} q(t) + N^T q(t) \tag{14}$$

Using Equations (10), (12), (13) and (14) in Equation (3), we get

$$C_1^T \left(I + \frac{1}{T_2} I^{(\alpha)} \right) - w_0 C_2^T I^{(\beta)} = w_0 M^T - \frac{1}{T_2} L^T \tag{15}$$

$$w_0 C_1^T I^{(\alpha)} + C_2^T \left(I + \frac{1}{T_2} I^{(\beta)} \right) = -w_0 L^T - \frac{1}{T_2} M^T \tag{16}$$

$$C_3^T \left(I + \frac{1}{T_1} I^{(\gamma)} \right) = O^T - \frac{1}{T_1} N^T \tag{17}$$

where $I^{(\alpha)}$, $I^{(\beta)}$ and $I^{(\gamma)}$ are the operational matrices of non-integer-order integration of order α, β and γ , respectively. Here I is an identity matrix.

The simpler form for Equations (15)–(17) is given as follows:

$$C_1^T W_1 - C_2^T W_5 = G_1, \tag{18}$$

$$C_1^T W_4 + C_2^T W_2 = G_2, \tag{19}$$

$$C_3^T W_3 = G_3, \tag{20}$$

where

$$W_1 = I + \frac{1}{T_2} I^{(\alpha)}, \tag{21}$$

$$W_2 = I + \frac{1}{T_2} I^{(\beta)}, \tag{22}$$

$$W_3 = I + \frac{1}{T_1} I^{(\gamma)}, \tag{23}$$

$$W_4 = w_0 I^{(\alpha)}, \tag{24}$$

$$W_5 = w_0 I^{(\beta)}, \tag{25}$$

$$G_1 = w_0 M^T - \frac{1}{T_2} L^T, \tag{26}$$

$$G_2 = -w_0 L^T - \frac{1}{T_2} M^T, \tag{27}$$

$$G_3 = O^T - \frac{1}{T_1} N^T \tag{28}$$

The matrices $W_1, W_2, W_3, W_4, W_5, G_1, G_2$ and G_3 are given in terms of known values, so these matrices are known matrices.

On solving Equations (18)–(20), we get

$$C_1^T = (G_1 W_5^{-1} + G_2 W_2^{-1}) (W_1 W_5^{-1} + W_4 W_2^{-1})^{-1}, \tag{29}$$

$$C_2^T = \left\{ (G_1 W_5^{-1} + G_2 W_2^{-1}) (W_1 W_5^{-1} + W_4 W_2^{-1})^{-1} W_1 - G_1 \right\} W_5^{-1}, \tag{30}$$

$$C_3^T = G_3 W_3^{-1} \tag{31}$$

Using Equations (29)–(31) in Equations (12)–(14), respectively, we get the system magnetisation $N_x(t)$, $N_y(t)$ and $N_z(t)$ for Bloch equations in NMR.

4. Convergence Analysis

Theorem 2. If $\frac{d^\alpha N_x}{dt^\alpha} \in C^{(m+1)}[0, 1]$ and $R_m\left(\frac{d^\alpha N_x}{dt^\alpha}\right)$ are the m^{th} approximations of $\frac{d^\alpha N_x}{dt^\alpha}$ by using $P_m(t) = span\{\sigma_0(t), \sigma_1(t), \dots, \sigma_m(t)\}$, then $\lim_{m \rightarrow \infty} \left\| \frac{d^\alpha N_x}{dt^\alpha} - R_m\left(\frac{d^\alpha N_x}{dt^\alpha}\right) \right\|_{w(a,b)} \rightarrow 0$.

Proof. Since $\frac{d^\alpha N_x}{dt^\alpha} \in C^{(m+1)}[0, 1]$, so the Taylor polynomial of $\frac{d^\alpha N_x}{dt^\alpha}$ at $t = 0$ is given as follows:

$$M_1(t) = \left(\frac{d^\alpha N_x}{dt^\alpha}\right)_{t=0} + \left(\frac{d^\alpha N_x}{dt^\alpha}\right)'_{t=0} t + \dots + \left(\frac{d^\alpha N_x}{dt^\alpha}\right)^m_{t=0} \frac{t^m}{m!}. \tag{32}$$

The upper bound of the error of the Taylor polynomial is given by

$$\left| \frac{d^\alpha N_x}{dt^\alpha} - M_1(t) \right| \leq \frac{K t^{m+1}}{(m+1)!}, \tag{33}$$

where

$$K = \max_{t \in [0,1]} \left| \left(\frac{d^\alpha N_x}{dt^\alpha}\right)^{m+1}(t) \right| \tag{34}$$

Since $R_m\left(\frac{d^\alpha N_x}{dt^\alpha}\right)$ and $M_1 \in P_m$, we have

$$\begin{aligned} \left\| \frac{d^\alpha N_x}{dt^\alpha} - R_m\left(\frac{d^\alpha N_x}{dt^\alpha}\right) \right\|_{w(a,b)}^2 &\leq \left\| \frac{d^\alpha N_x}{dt^\alpha} - M_1 \right\|_{w(a,b)}^2 \\ &\leq \left(\frac{K}{(m+1)!}\right)^2 \int_0^1 t^{2m+2+b} (1-t)^a dt, \\ &= \left(\frac{K}{(m+1)!}\right)^2 \frac{(1+a)(3+2m+b)}{(4+2m+a+b)}, \\ \left\| \frac{d^\alpha N_x}{dt^\alpha} - R_m\left(\frac{d^\alpha N_x}{dt^\alpha}\right) \right\|_{w(a,b)} &\leq \frac{K}{(m+1)!} \sqrt{\frac{(1+a)(3+2m+b)}{(4+2m+a+b)}} \end{aligned} \tag{35}$$

Taking $m \rightarrow \infty$ in Equation (35), we get

$$\lim_{m \rightarrow \infty} \left\| \frac{d^\alpha N_x}{dt^\alpha} - R_m\left(\frac{d^\alpha N_x}{dt^\alpha}\right) \right\|_{w(a,b)} \rightarrow 0. \square$$

5. Numerical Results and Discussion

In this section, we will numerically simulate our results with known results. For each numerical simulation, we will consider i. c. $N_x(0) = 0$, $N_y(0) = 100$ and $N_z(0) = 0$. In Figures 1 and 2, we have presented 3D and 2D plots of the numerical solutions of the Bloch equation for integer order, respectively. These figures show the dynamics of N_x , N_y and N_z for integer-order relaxation. In Figure 1, the entire trajectory of magnetisation is shown in 3D for integer order starting at i. c. $(N_x(0), N_y(0), N_z(0))$ and returning to N_0 . From Figure 2, it is clear that the magnetisation N_x in x -direction increases with time, and the magnetisation N_y in y -direction decreases with time.

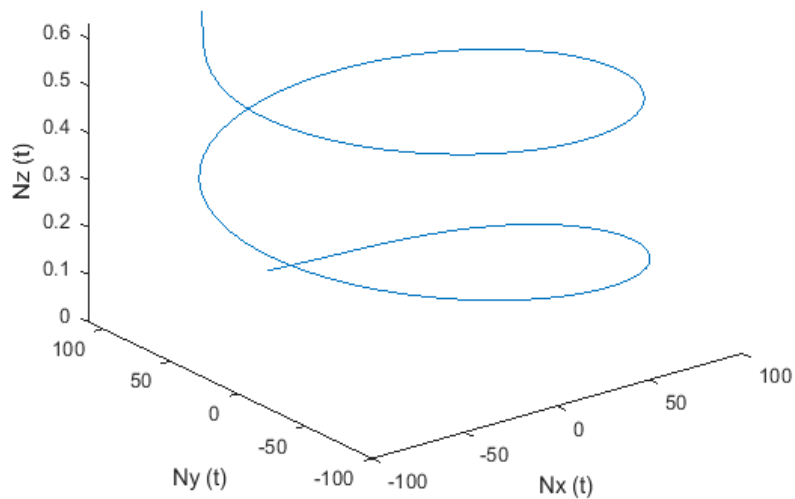


Figure 1. Numerical solutions of the Bloch equation with parameters: $\alpha = \beta = \gamma = 1, w_0 = 12, T_1 = 1, T_2 = 20, a = 1, b = 1$.

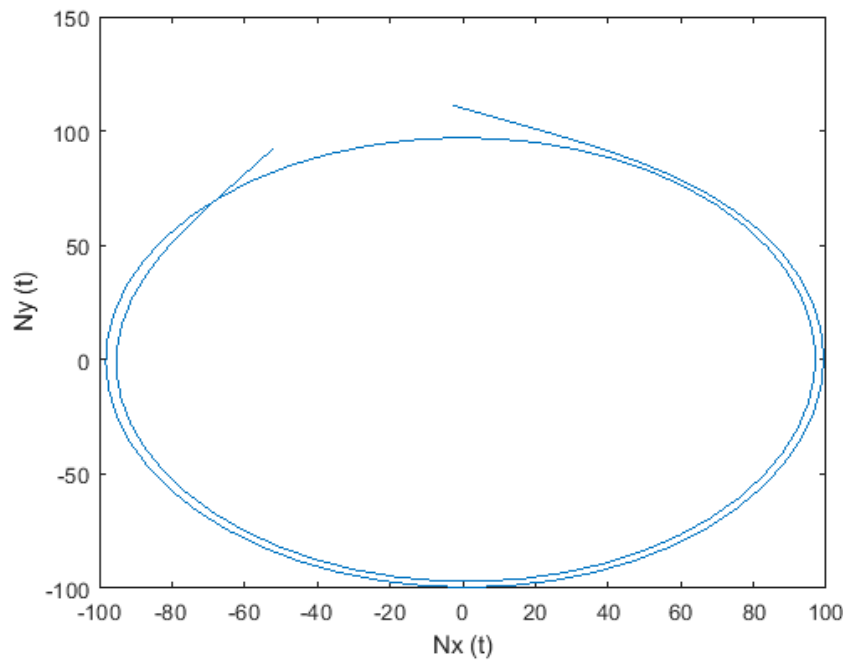


Figure 2. Numerical solutions of the Bloch equation in plane (N_x vs. N_y) with parameters: $\alpha = \beta = \gamma = 1, w_0 = 12, T_1 = 1, T_2 = 20, a = 1, b = 1$.

In Figures 3 and 4, we have presented 3D and 2D plots of the numerical solutions of the Bloch equation for fractional order ($\alpha = \beta = \gamma = 0.9$), respectively. These figures show the dynamics of N_x, N_y and N_z for fractional-order relaxation. In Figure 3, the entire trajectory of magnetisation is shown in 3D for fractional order ($\alpha = \beta = \gamma = 0.9$) starting at i. c. $(N_x(0), N_y(0), N_z(0))$ and returning to N_0 . From Figure 4, it is clear that the magnetisation N_x in x -direction increases with time, and the magnetisation N_y in y -direction decreases with time.

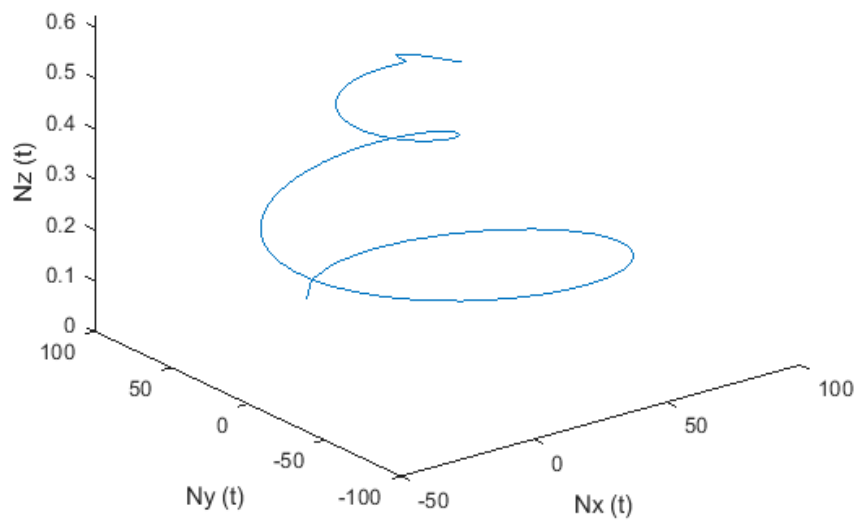


Figure 3. Numerical solutions of the Bloch equation with parameters: $\alpha = \beta = \gamma = 0.9$, $w_0 = 12$, $T_1 = 1$, $T_2 = 20$, $a = 1$, $b = 1$.

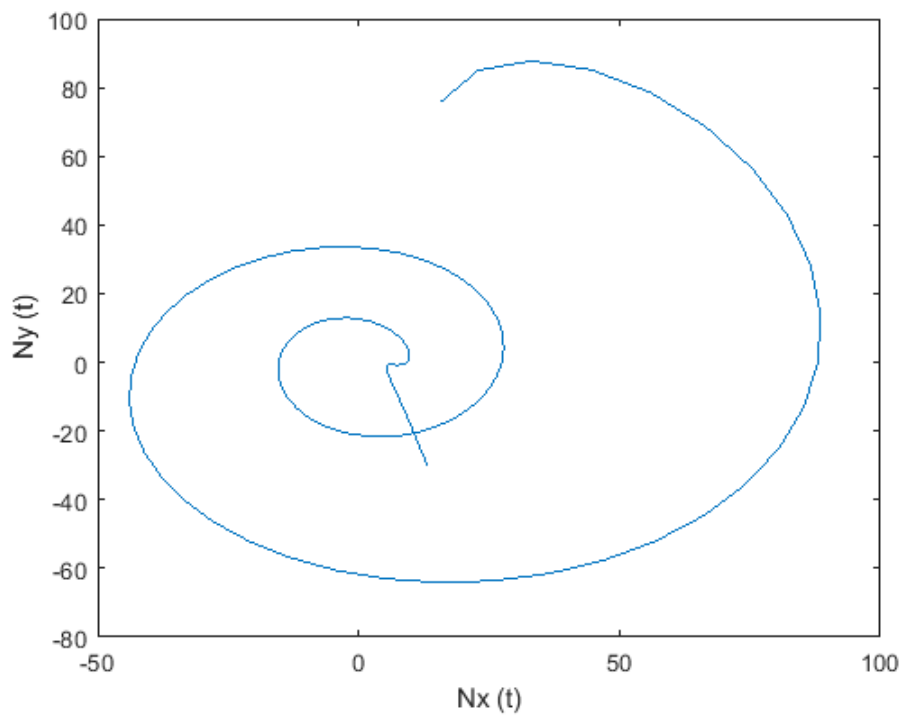


Figure 4. Numerical solutions of the Bloch equation in the plane (N_x vs. N_y) with parameters: $\alpha = \beta = \gamma = 0.9$, $w_0 = 12$, $T_1 = 1$, $T_2 = 20$, $a = 1$, $b = 1$.

In Figures 5 and 6, we have presented the 3D and 2D plots of the numerical solutions of the Bloch equation for fractional order ($\alpha = \beta = \gamma = 0.8$), respectively. These figures show the dynamics of N_x , N_y and N_z for the fractional-order relaxation. In Figure 5, the entire trajectory of magnetisation is shown in 3D for fractional order ($\alpha = \beta = \gamma = 0.8$) starting at i. c. $(N_x(0), N_y(0), N_z(0))$ and returning to N_0 . From Figure 6, it is clear that the magnetisation N_x in x -direction increases with time, and the magnetisation N_y in y -direction decreases with time.

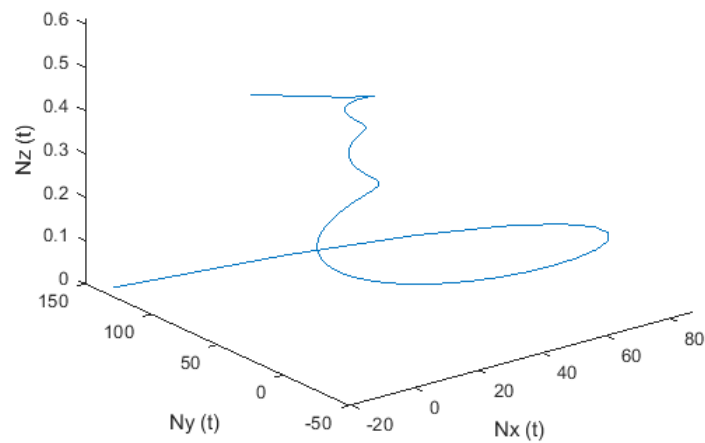


Figure 5. Numerical solutions of the Bloch equation with parameters: $\alpha = \beta = \gamma = 0.8$, $w_0 = 12$, $T_1 = 1$, $T_2 = 20$, $a = 1$, $b = 1$.

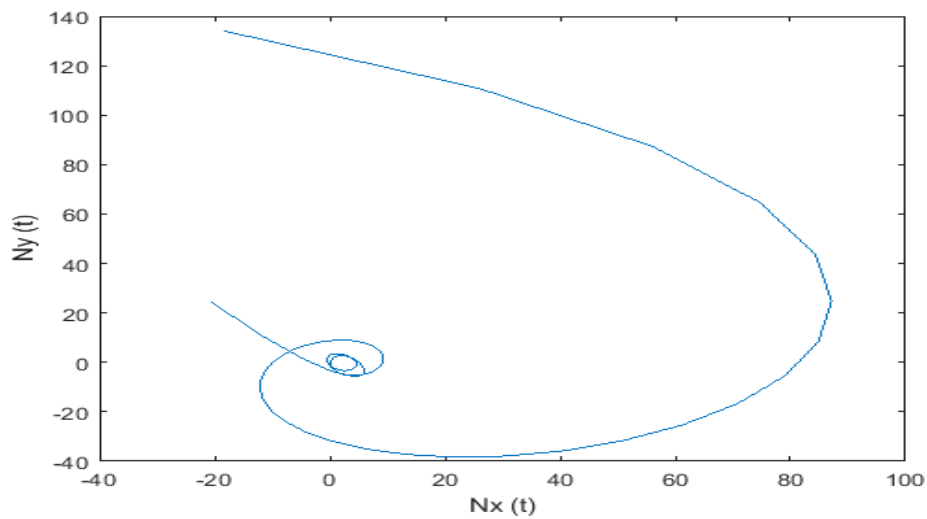


Figure 6. Numerical solutions of the Bloch equation in the plane (N_x vs. N_y) with parameters: $\alpha = \beta = \gamma = 0.8$, $w_0 = 12$, $T_1 = 1$, $T_2 = 20$, $a = 1$, $b = 1$.

In Figures 7 and 8, we have presented the 3D and 2D plots of the numerical solutions of the Bloch equation for fractional order ($\alpha = \beta = \gamma = 0.7$), respectively. These figures show the dynamics of N_x , N_y and N_z for the fractional-order relaxation. In Figure 7, the entire trajectory of magnetisation is shown in 3D for fractional order ($\alpha = \beta = \gamma = 0.7$) with the starting initially $(N_x(0), N_y(0), N_z(0))$ and returning to N_0 . From Figure 8, it is clear that the magnetisation N_x in x -direction increases with time, and the magnetisation N_y in y -direction decreases with time.

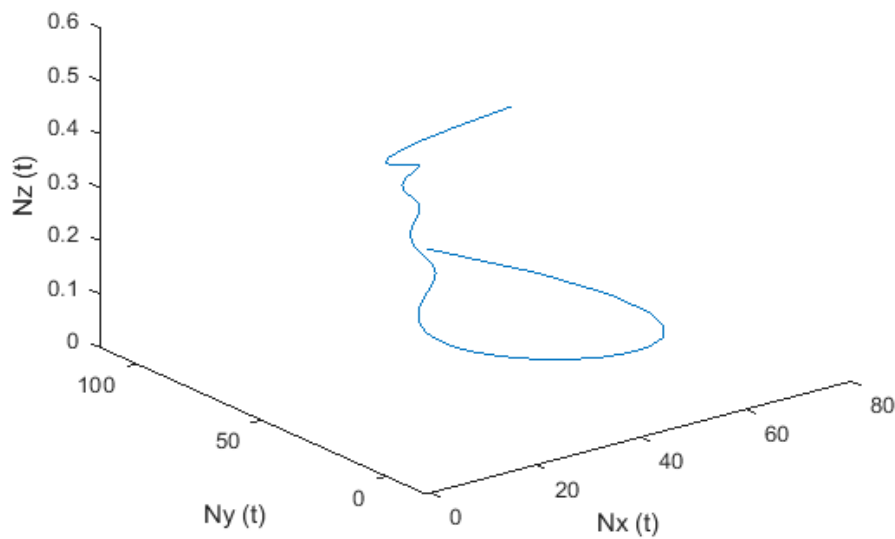


Figure 7. Numerical solutions of the Bloch equation with parameters: $\alpha = \beta = \gamma = 0.7$, $w_0 = 12$, $T_1 = 1$, $T_2 = 20$, $a = 1$, $b = 1$.

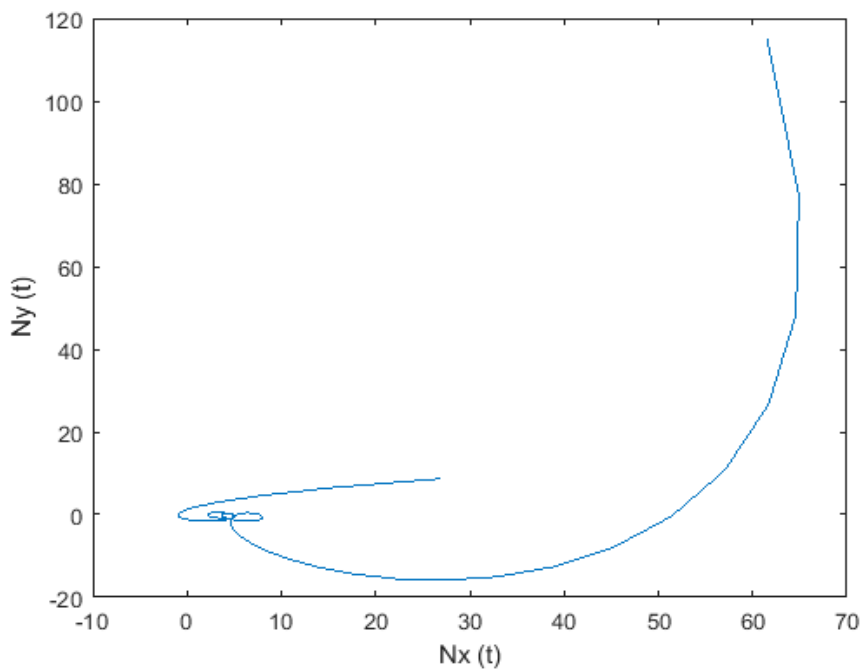


Figure 8. Numerical solutions of the Bloch equation in the plane (N_x vs. N_y) with parameters: $\alpha = \beta = \gamma = 0.7$, $w_0 = 12$, $T_1 = 1$, $T_2 = 20$, $a = 1$, $b = 1$.

In Figures 9 and 10, we have presented the 3D and 2D plots of the numerical solutions of the Bloch equation for fractional order ($\alpha = 1.0$, $\beta = 0.9$, $\gamma = 0.8$), respectively. These figures show the dynamics of N_x , N_y and N_z for the fractional-order relaxation. In Figure 9, the entire trajectory of magnetisation is shown in 3D for fractional order ($\alpha = 1.0$, $\beta = 0.9$, $\gamma = 0.8$) starting at i. c. $(N_x(0), N_y(0), N_z(0))$ and returning to N_0 . From Figure 10, it is clear that the magnetisation N_x in x -direction increases with time, and the magnetisation N_y in y -direction decreases with time.

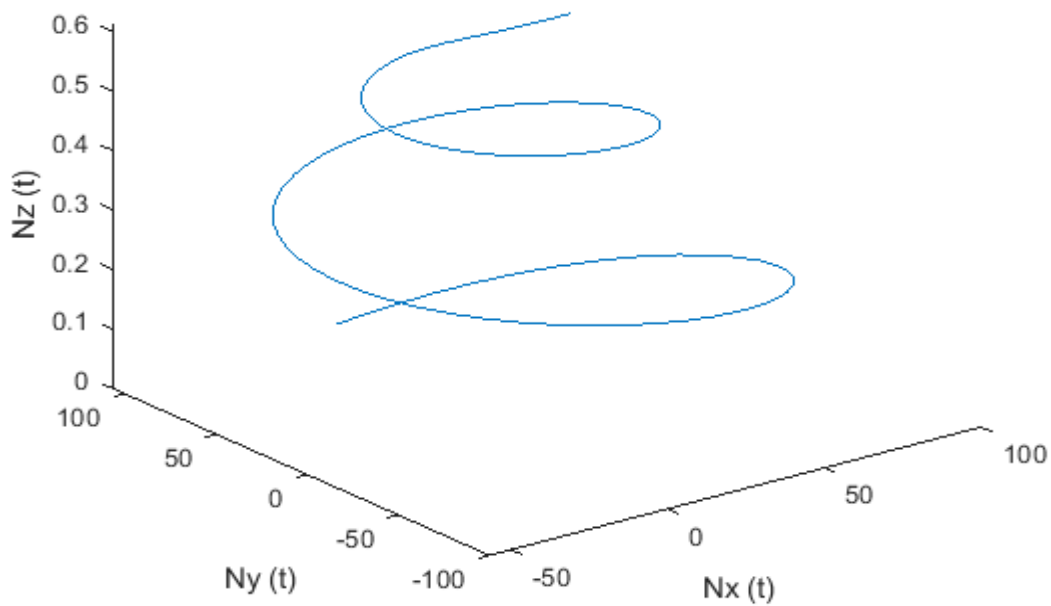


Figure 9. Numerical solutions of the Bloch equation with parameters: $\alpha = 1.0, \beta = 0.9, \gamma = 0.8, w_0 = 12, T_1 = 1, T_2 = 20, a = 1, b = 1$.

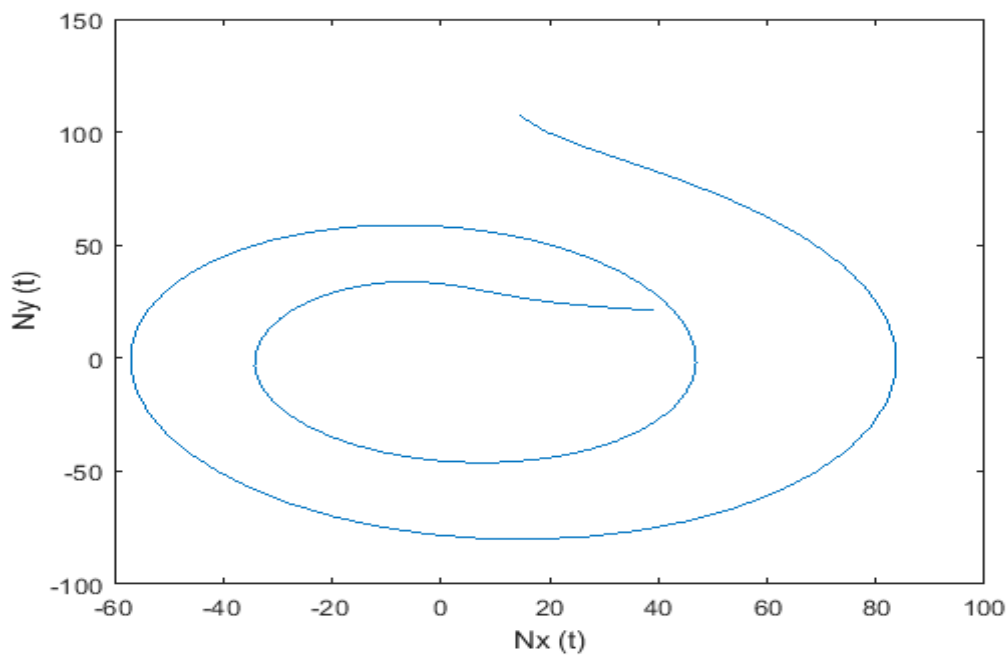


Figure 10. Numerical solutions of the Bloch equation in the plane (N_x vs. N_y) with parameters: $\alpha = 1.0, \beta = 0.9, \gamma = 0.8, w_0 = 12, T_1 = 1, T_2 = 20, a = 1, b = 1$.

In Figures 11 and 12 we have presented 3D and 2D plots of numerical solutions of Bloch equation for fractional order ($\alpha = 0.9, \beta = 0.9, \gamma = 1.0$), respectively. These figures show the dynamic of N_x, N_y and N_z for fractional order relaxation. In Figure 11, the entire trajectory of magnetisation is shown in 3D for fractional order ($\alpha = 0.9, \beta = 0.9, \gamma = 1.0$) starting at i.c. $(N_x(0), N_y(0), N_z(0))$ and returning to N_0 . From Figure 12, it is clear that the magnetisation N_x in x -direction increases with time, and the magnetisation N_y in y -direction decreases with time.

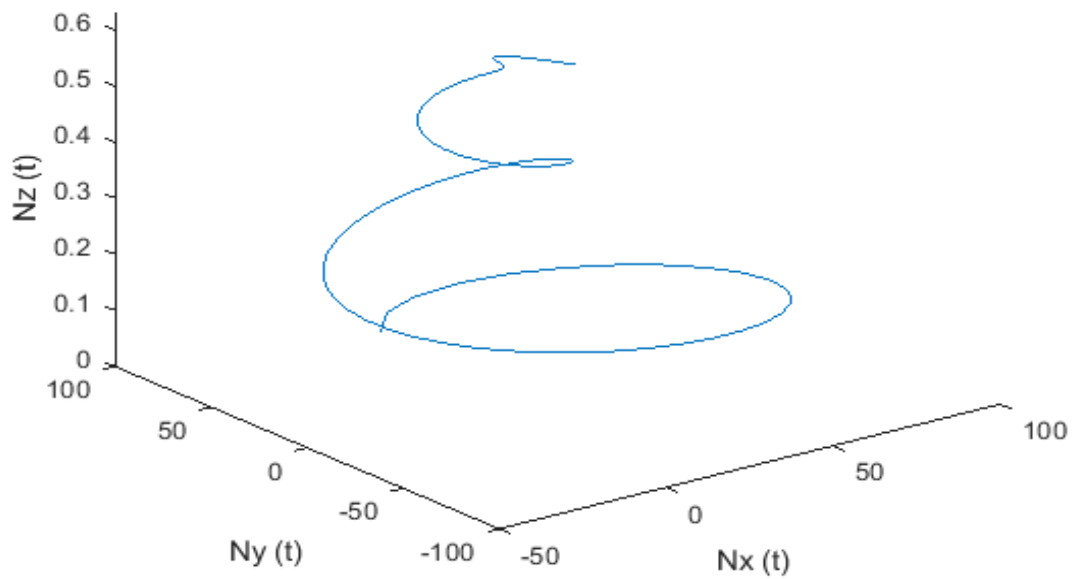


Figure 11. Numerical solutions of the Bloch equation with parameters: $\alpha = 0.9$, $\beta = 0.9$, $\gamma = 1$, $w_0 = 12$, $T_1 = 1$, $T_2 = 20$, $a = 1$, $b = 1$.

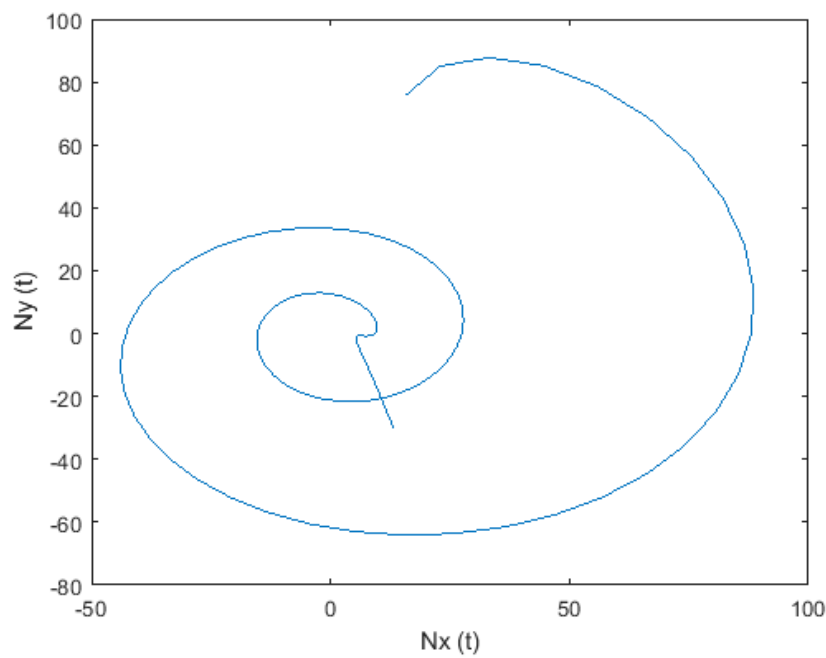


Figure 12. Numerical solutions of the Bloch equation in the plane (N_x vs. N_y) with parameters: $\alpha = 0.9$, $\beta = 0.9$, $\gamma = 1$, $w_0 = 12$, $T_1 = 1$, $T_2 = 20$, $a = 1$, $b = 1$.

In Figures 13 and 14, we have presented the 3D and 2D plots of the numerical solutions of the Bloch equation for fractional order ($\alpha = 1.0$, $\beta = 1.0$, $\gamma = 0.9$), respectively. These figures show the dynamics of N_x , N_y and N_z for the fractional-order relaxation. In Figure 13, the entire trajectory of magnetisation is shown in 3D for fractional order ($\alpha = 1.0$, $\beta = 1.0$, $\gamma = 0.9$) starting at the initial level $(N_x(0), N_y(0), N_z(0))$ and returning to N_0 . From Figure 14, it is clear that the magnetisation N_x in x -direction increases with time, and the magnetisation N_y in y -direction decreases with time.

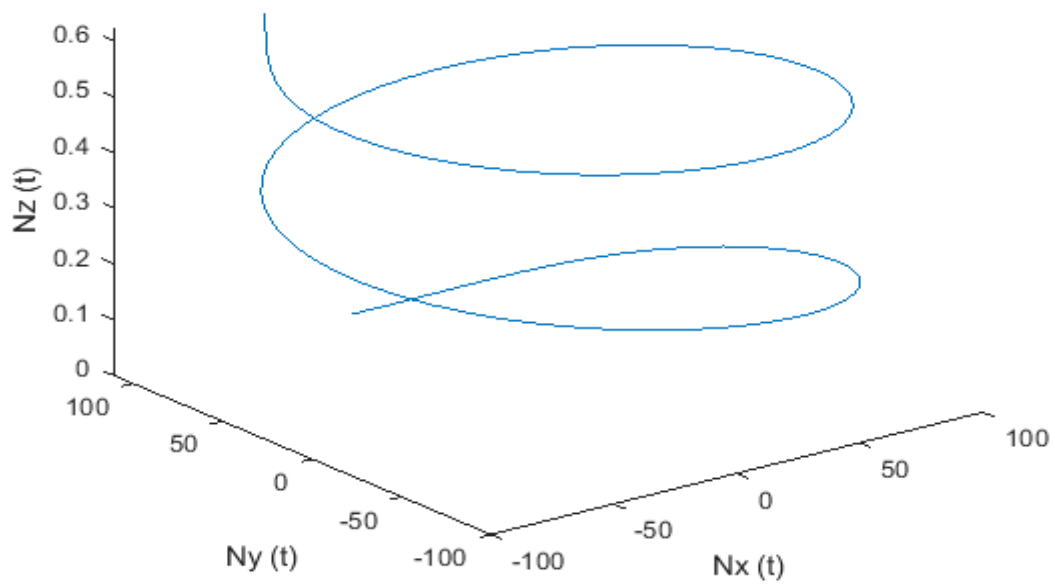


Figure 13. Numerical solutions of the Bloch equation with parameters: $\alpha = 1, \beta = 1, \gamma = 0.9, w_0 = 12, T_1 = 1, T_2 = 20, a = 1, b = 1$.

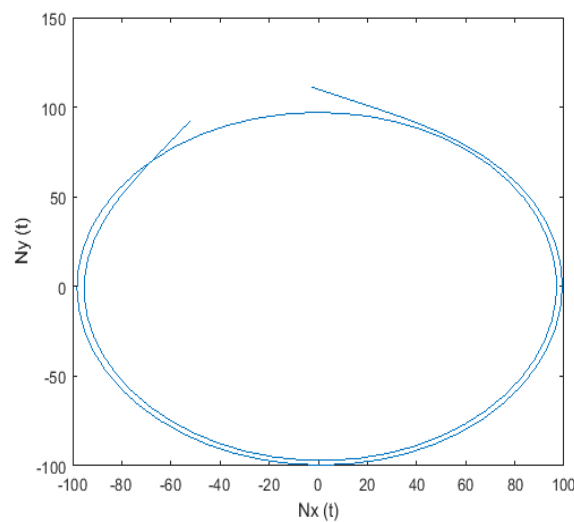


Figure 14. Numerical solutions of the Bloch equation in the plane (N_x vs. N_y) with parameters: $\alpha = 1, \beta = 1, \gamma = 0.9, w_0 = 12, T_1 = 1, T_2 = 20, a = 1, b = 1$.

In Figures 15 and 16, we have shown the numerical simulation of analytical and numerical solutions of the Bloch equation for $N_x(t)$ and $N_y(t)$ for integer order, respectively. From Figure 16, it is clear that the solution has periodic behaviour at low frequency. This solution varies periodically for $N_x(t)$ and $N_y(t)$ at low frequency.

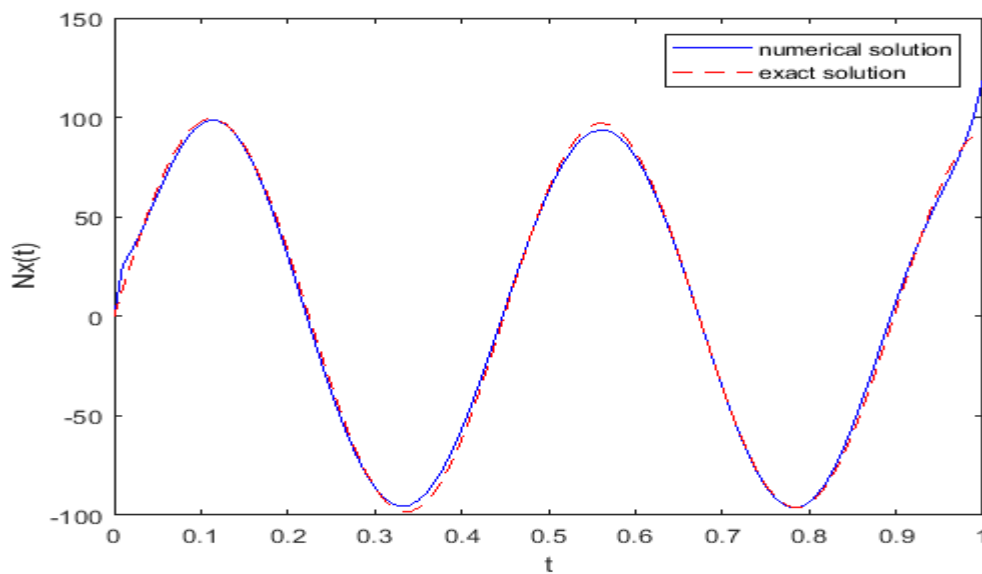


Figure 15. Numerical simulation of solutions of the Bloch equation for $N_x(t)$ with parameters: $\alpha = \beta = \gamma = 1, w_0 = 14, T_1 = 1, T_2 = 20, a = 0.9, b = 0.9$.

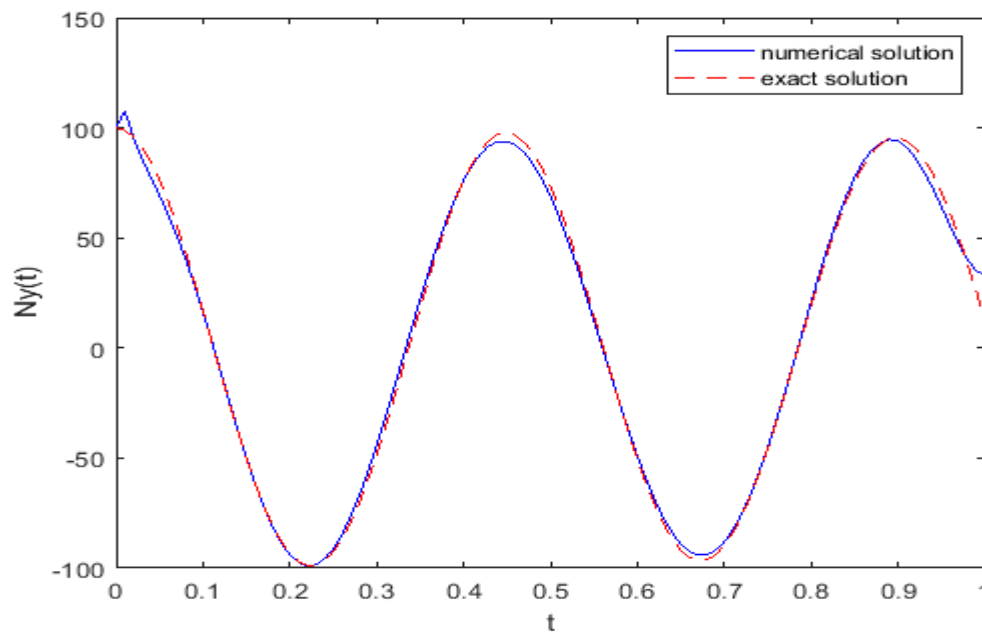


Figure 16. Numerical simulation of solutions of the Bloch equation for $N_y(t)$ with parameters: $\alpha = \beta = \gamma = 1, w_0 = 14, T_1 = 1, T_2 = 20, a = 0.9, b = 0.9$.

In Figures 17–19, we have shown the absolute errors for $N_x(t)$, $N_y(t)$ and $N_z(t)$, respectively, at different values of $m = 3, 6$ and 9 . In Figures 17–19, the absolute errors are denoted by E_1, E_2 and E_3 for $m = 3, 6$ and 9 , respectively. In all these figures, E_2 and E_3 are multiplied by 10^4 and 10^5 , respectively.

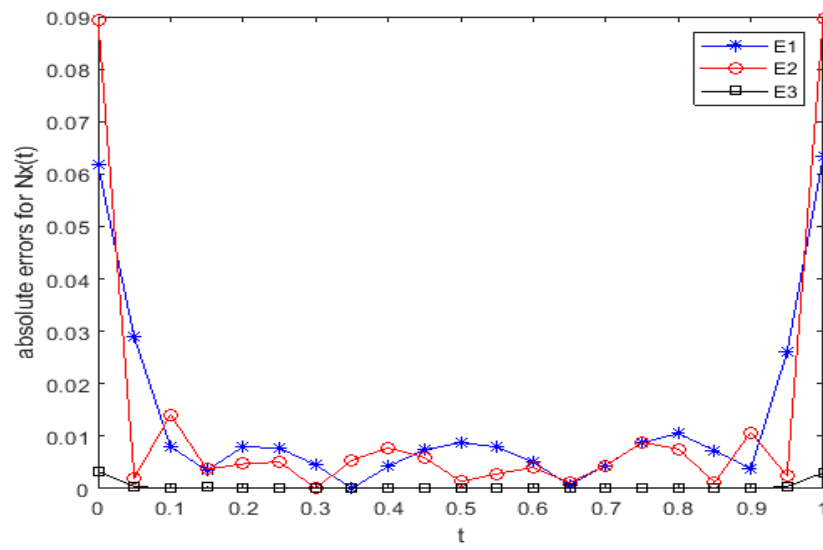


Figure 17. Errors for $N_x(t)$ at $m = 3, 6$ and 9 , with parameters: $\alpha = \beta = \gamma = 1, w_0 = 1, T_1 = 1, T_2 = 20, a = 1, b = 1$.

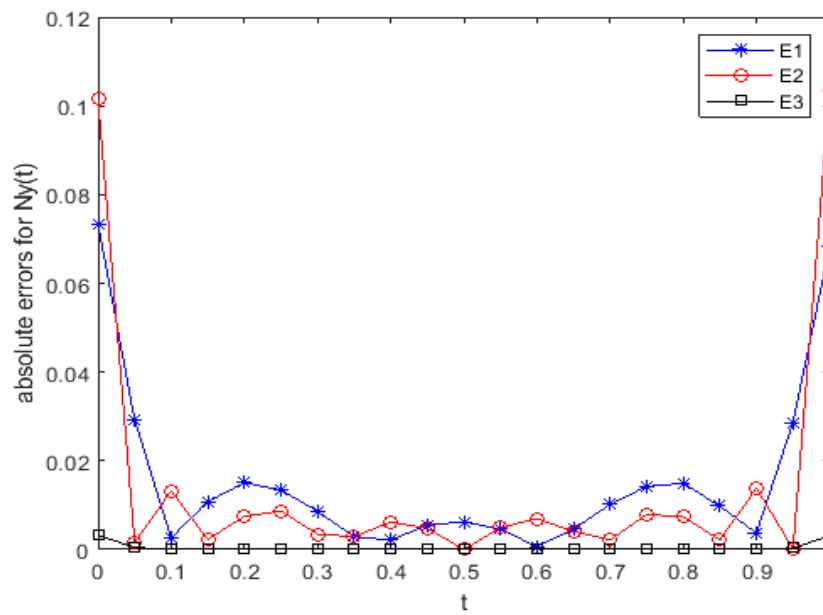


Figure 18. Errors for $N_y(t)$ at $m = 3, 6$ and 9 , with parameters: $\alpha = \beta = \gamma = 1, w_0 = 1, T_1 = 1, T_2 = 20, a = 1, b = 1$.

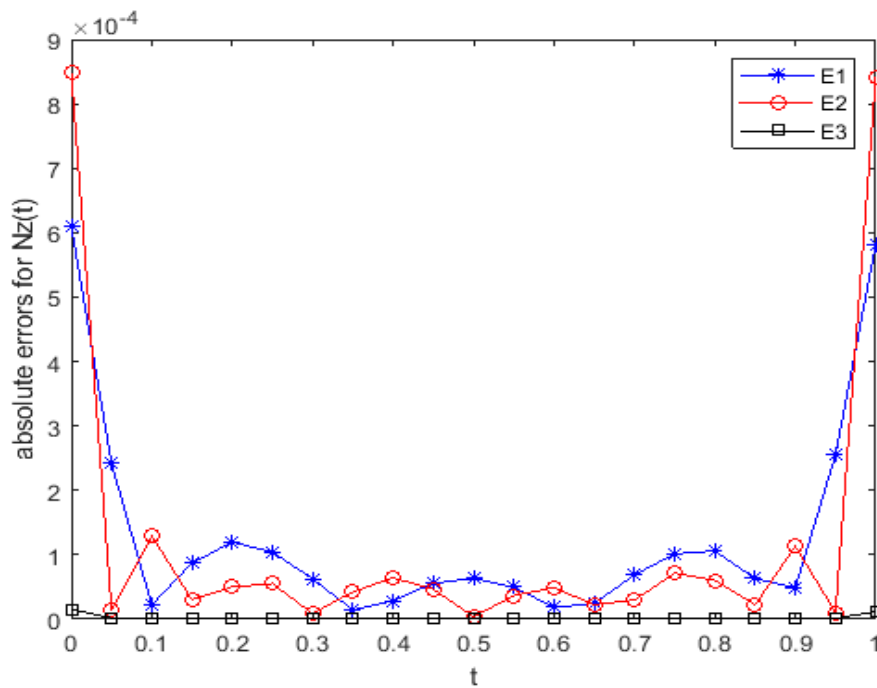


Figure 19. Errors for $N_z(t)$ at $m = 3, 6$ and 9 , with parameters: $\alpha = \beta = \gamma = 1, w_0 = 1, T_1 = 1, T_2 = 20, a = 1, b = 1$.

From these figures, we can see that the errors decrease with the increase of m . In Figures 20–22, we have shown the behaviour of the solutions of $N_x(t), N_y(t)$ and $N_z(t)$ at different values of α, β and γ , respectively. In Figures 20–22, exact solution means the analytical solution for integer order ($\alpha = \beta = \gamma = 1$) Bloch equation as given by Equation (2).

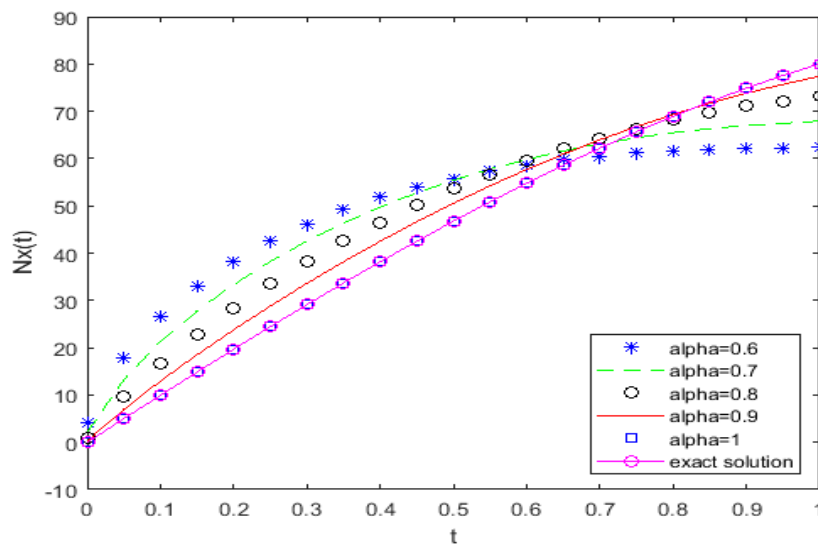


Figure 20. Behaviour of the approximate solution of $N_x(t)$ at $\alpha = 0.6, 0.7, 0.8, 0.9$ and 1 , with parameters: $w_0 = 1, T_1 = 1, T_2 = 20, a = 1, b = 1$.

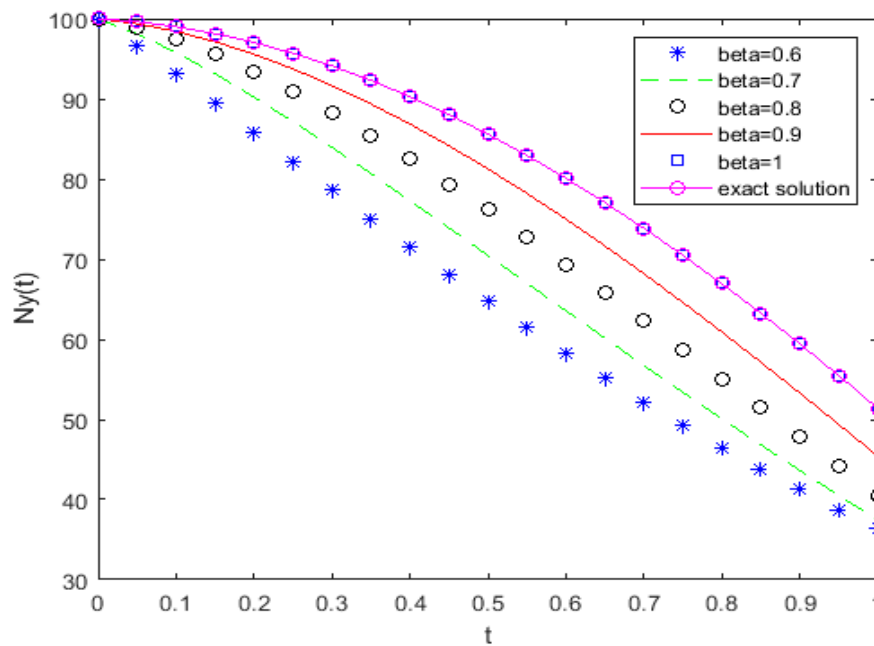


Figure 21. Behaviour of the approximate solution of $N_y(t)$ at $\beta = 0.6, 0.7, 0.8, 0.9$ and 1 , with parameters: $w_0 = 1, T_1 = 1, T_2 = 20, a = 1, b = 1$.

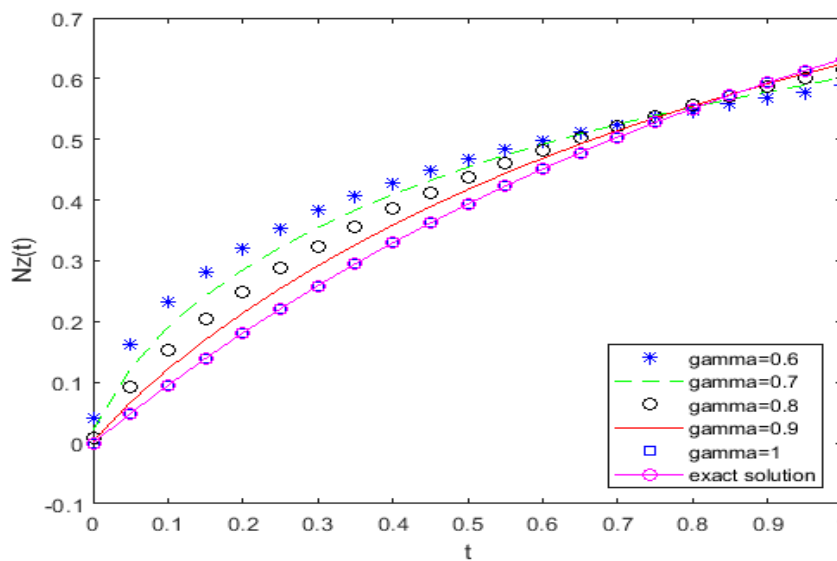


Figure 22. Behaviour of the approximate solution of $N_z(t)$ at $\gamma = 0.6, 0.7, 0.8, 0.9$ and 1 , with parameters: $w_0 = 1, T_1 = 1, T_2 = 20, a = 1, b = 1$.

From these figures it is clear that the solution varies consistently from non-integer order to integer order.

In Table 1, we have listed the maximum absolute errors (I^∞) and the root-mean-square errors (I^2) for two different values of $m = 4$ and 8 at $\alpha = \beta = \gamma = 1, w_0 = 1, T_1 = 1, T_2 = 20, a = b = 0.8$. We have calculated these errors for integer order by taking the exact solution as given by Equation (2).

Table 1. Comparison of (l^∞) and (l^2) errors at $a = b = 0.8$, $m = 5, 8$ for integer order solution.

$N_i(t)$	$m = 5$	$m = 8$
	l^∞ -Error l^2 -Error	l^∞ -Error l^2 -Error
$N_x(t)$	2.0349×10^{-4}	4.2101×10^{-8}
	5.7209×10^{-6}	9.2050×10^{-10}
$N_y(t)$	1.9648×10^{-4}	6.2953×10^{-10}
	5.5559×10^{-6}	6.2953×10^{-10}
$N_z(t)$	1.7733×10^{-6}	5.7426×10^{-10}
	5.0010×10^{-8}	6.8075×10^{-12}

From Table 1, it is detected that the errors decrease with the increase of m .

6. Conclusions and Future Scope

In this paper, we have presented the numerical solution and the simulation for fractional-order and integer-order Bloch equations. Mathematical model for NMR allows us to explore and define magnetisation for spin dynamics at resonance frequency in a static magnetic field. Implementation of our proposed technique is easy in comparison to the existing methods because the operational matrices are easy to construct. The numerical section shows how the solution given by the used technique varies consistently at different values of non-integer-order time-derivatives. Moreover, for integer order, the solution by the used technique is identical to the exact solution for the Bloch equation. The error table shows the accuracy of the proposed method. For future work, we can construct operational matrices for different polynomials in order to attain better exactness.

Author Contributions: Both authors have equal contribution. All authors have read and agreed to the published version of the manuscript.

Funding: This research received no external funding.

Conflicts of Interest: The authors declare no conflict of interest.

References

1. Bagley, R.L.; Torvik, P.J. A theoretical basis for the application of fractional calculus to viscoelasticity. *J. Rheol.* **1983**, *27*, 201–210. [[CrossRef](#)]
2. Srivastava, H.M.; Shah, F.A.; Abass, R. An application of the Gegenbauer wavelet method for the numerical solution of the fractional Bagley-Torvik equation. *Russ. J. Math. Phys.* **2019**, *26*, 77–93. [[CrossRef](#)]
3. Bagley, R.L.; Torvik, P.J. Fractional calculus in the transient analysis of viscoelasticity damped structures. *AIAA J.* **1985**, *23*, 918–925. [[CrossRef](#)]
4. Robinson, A.D. The use of control systems analysis in neurophysiology of eye movements. *Annu. Rev. Neurosci.* **1981**, *4*, 462–503. [[CrossRef](#)] [[PubMed](#)]
5. Singh, H. A new stable algorithm for fractional Navier-Stokes equation in polar coordinate. *Int. J. Appl. Comput. Math.* **2017**, *3*, 3705–3722. [[CrossRef](#)]
6. Bohannan, G.W. Analog fractional order controller in temperature and motor control applications. *J. Vib. Control* **2008**, *14*, 1487–1498. [[CrossRef](#)]
7. Panda, R.; Dash, M. Fractional generalized splines and signal processing. *Signal Process* **2006**, *86*, 2340–2350. [[CrossRef](#)]
8. Kilbas, A.A.; Srivastava, H.M.; Trujillo, J.J. *Theory and Applications of Fractional Differential Equations, North-Holland Mathematical Studies*; Elsevier (North-Holland) Science Publishers: Amsterdam, The Netherlands, 2006.
9. Li, X. Numerical solution of fractional partial differential equations using cubic B-spline wavelet collocation method. *Adv. Comput. Math. Appl.* **2012**, *1*, 159–164.
10. Daftardar-Gejji, V.; Bhalekar, S. Solving fractional diffusion-wave equations using a new iterative method. *Fract. Calc. Appl. Anal.* **2008**, *11*, 193–202.

11. Awojoyogber, O.B. Analytical solution of the time dependent Bloch NMR, flow equations: A translational mechanical analysis. *Phys. A Stat. Mech. Appl.* **2004**, *339*, 437–460. [[CrossRef](#)]
12. Murase, K.; Tanki, N. Numerical solution to the time dependent Bloch equations revisited. *Magn. Reson. Imaging* **2011**, *29*, 126–131. [[CrossRef](#)] [[PubMed](#)]
13. Leyte, J.C. Some solutions of the Bloch equations. *Chem. Phys. Lett.* **1990**, *165*, 231–240. [[CrossRef](#)]
14. Yan, H.; Chen, B.; Gore, J.C. Approximate solutions of the Bloch equations for selective excitation. *J. Magn. Reson.* **1987**, *75*, 83–95. [[CrossRef](#)]
15. Hoult, D.I. The solution of the Bloch equation in presence of varying B₁ field—An approach to selective pulse analysis. *J. Magn. Reson.* **1979**, *35*, 69–86. [[CrossRef](#)]
16. Xu, Z.; Chan, A.K. A Near-Resonance solution to the Bloch equations and its application to RF pulse design. *J. Magn. Reson.* **1999**, *138*, 225–231. [[CrossRef](#)]
17. Magin, R.; Feng, X.; Baleanu, D. Solving the fractional order Bloch Equation. *Concepts Magn. Reson. Part A* **2009**, *34*, 16–23. [[CrossRef](#)]
18. Kumar, S.; Faraz, N.; Sayevand, K. A fractional model of Bloch equation in NMR and its analytic approximate solution. *Walailak J. Sci. Technol.* **2014**, *11*, 273–285.
19. Singh, H. A New Numerical Algorithm for Fractional Model of Bloch equation in nuclear magnetic resonance. *Alex. Eng. J.* **2016**, *55*, 2863–2869. [[CrossRef](#)]
20. Singh, H. Operational matrix approach for approximate solution of fractional model of Bloch equation. *J. King Saud Univ. Sci.* **2017**, *29*, 235–240. [[CrossRef](#)]
21. Petráš, L. Modeling and numerical analysis of fractional-order Bloch equations. *Comput. Math. Appl.* **2011**, *61*, 341–356. [[CrossRef](#)]
22. Ahmadian, A.; Chan, C.S.; Salahshour, S.; Vaitheeswaran, V. FTFBE: A numerical approximation for fuzzy time-fractional Bloch equation. In Proceedings of the International conference on fuzzy systems (FUZZ-IEEE), World Congress on Computational Intelligence, Beijing, China, 6–11 July 2014; pp. 418–423.
23. Wu, J.L. A wavelet operational method for solving fractional partial differential equations numerically. *Appl. Math. Comput.* **2009**, *214*, 31–40. [[CrossRef](#)]
24. Singh, H.; Srivastava, H.M.; Kumar, D. A reliable numerical algorithm for the fractional vibration equation. *Chaos Solitons Fractals* **2017**, *103*, 131–138. [[CrossRef](#)]
25. Tohidi, E.; Bhrawy, A.H.; Erfani, K. A collocation method based on Bernoulli operational matrix for numerical solution of generalized pantograph equation. *Appl. Math. Model.* **2013**, *37*, 4283–4294. [[CrossRef](#)]
26. Kazem, S.; Abbasbandy, S.; Kumar, S. Fractional order Legendre functions for solving fractional-order differential equations. *Appl. Math. Model.* **2013**, *37*, 5498–5510. [[CrossRef](#)]
27. Singh, C.S.; Singh, H.; Singh, V.K.; Singh, O.P. Fractional order operational matrix methods for fractional singular integro-differential equation. *Appl. Math. Model.* **2016**, *40*, 10705–10718. [[CrossRef](#)]
28. Singh, H.; Srivastava, H.M. Jacobi collocation method for the approximate solution of some fractional-order Riccati differential equations with variable coefficients. *Phys. A Stat. Mech. Appl.* **2019**, *523*, 1130–1149. [[CrossRef](#)]
29. Singh, C.S.; Singh, H.; Singh, S.; Kumar, D. An efficient computational method for solving system of nonlinear generalized Abel integral equations arising in astrophysics. *Phys. A Stat. Mech. Appl.* **2019**, *525*, 1440–1448. [[CrossRef](#)]
30. Singh, H.; Pandey, R.K.; Baleanu, D. Stable numerical approach for fractional delay differential equations. *Few-Body Syst.* **2017**, *58*, 156. [[CrossRef](#)]
31. Srivastava, H.M. Fractional-order derivatives and integrals: Introductory overview and recent developments. *Kyungpook Math. J.* **2020**, *60*, 73–116.

